Integrated Optics in Silicon and SiGe-Heterostructures

Bernd Schüppert, *Member, IEEE,* Joachim Schmidtchen, Armin Splett, *Member, IEEE,* Uwe Fischer, Thomas Zinke, Rudolf Moosburger, and Klaus Petermann, *Senior Member, IEEE*

(Invited Paper)

***Abstract*— This paper reviews various techniques and ideas in the field of integrated optics in silicon, mainly focused on silicon in conjunction with germanium. We will discuss different approaches for waveguides, passive and active components in silicon as well as recent developments in the fabrication and performance of such components. For waveguides in silicon, the characteristics such as losses and spot-sizes will be given, showing that silicon could be an attractive candidate for integrated optical devices.**

I. Introduction

SINCE silicon is the most commonly used material in semiconductor electronics it is commercially available in high quality at a low price. Hence, it is a logical step to investigate its optical properties and potential for integrated optical photonic devices [1] and [2] in order to use a material system which is entirely compatible with VLSI technology.

In today's integrated optics relatively complex devices are required, for example an integrated optical balanced receiver [3] and [4] for coherent optical communication systems (Fig. 1). Such devices always contain integrated optical waveguides as the most fundamental component and most probably passive components like bends and couplers and in some cases active components such as electro-optical switches and modulators. The monolithic integration of photodiodes is necessary in case of a coherent receiver in order to avoid signal-reflections at the photodiodes. Even though a monolithically integrated laser diode is preferrable, a hybrid mounted laser would be acceptable if the mounting technique is suitable for mass production. The design shown in Fig. 1 should be just considered as an artist's view, because in practice it suffers from the fact, that the etched adjustment grooves for the laser end at a $\langle 111 \rangle$-plane at an angle of 54.7° for $\langle 100 \rangle$-silicon, thus inhibiting light being coupled into the substrate. Appropriate solutions, however, will be discussed in the last section of this paper where we will deal with micromachined silicon.

A basic requirement for any optical application of a material is its transparency in the near infrared, i.e. at wavelengths of $\lambda = 1.3$ μm and/or $\lambda = 1.55$ μm. This basic condition is met by silicon, since it exhibits optical losses of less than 0.1 dB/cm in the near infrared regime at wavelengths of

Manuscript received January 5, 1996; revised July 1, 1996. This work was supported in part by Siemens AG and Volkswagen-Stiftung.

The authors are with Technische Universität Berlin, Fachgebiet Hochfrequenztechnik, Einsteinufer 25, D-10587 Berlin, Germany.

Publisher Item Identifier S 0733-8724(96)07680-3.

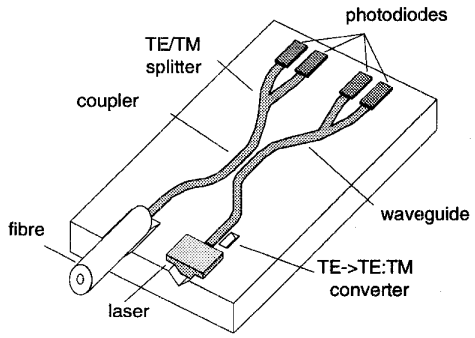

Fig. 1. Proposal for an integrated optical receiver for coherent optical systems.

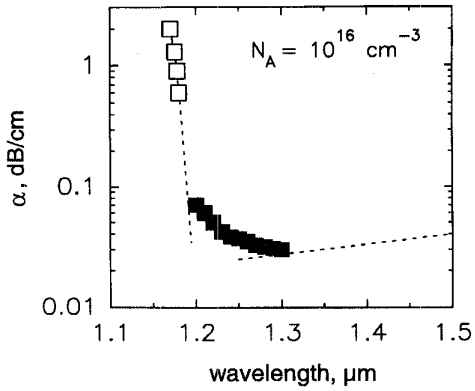

Fig. 2. Infrared absorption of silicon at $\lambda = 1.3$ μm [5].

$\lambda > 1.2$ μm as displayed in Fig. 2, showing the optical absorption against the wavelength in lightly doped silicon [5]. For low loss applications, the doping level must be low in order to avoid losses due to free carrier absorption, i.e. $N_{D,A} < 10^{17}$ cm^{-3} if additional losses should be below 1 dB/cm.

The intention of this paper is to review mainly the experimental and theoretical results obtained at Technical University of Berlin on SiGe/Si and silicon-on-insulator waveguide devices.

II. Waveguides

A basic requirement for a waveguide **in** silicon is a confinement of an optical wave in the vertical direction by means of a

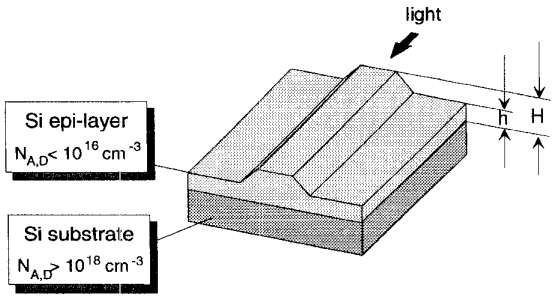

Fig. 3. Rib-waveguide in epitaxial silicon [5].

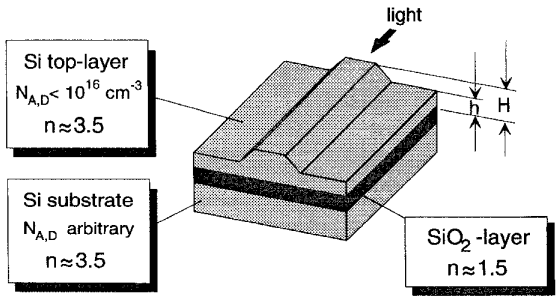

Fig. 4. Rib-waveguide in silicon-on-insulator (SOI).

refractive-index enhancement, which can be either step-like or smooth. Some waveguide concepts are based on an index step in the vertical direction of commercially available material, which is due to the incorporated layers, i.e., epitaxial silicon or silicon-on-insulator (SOI). Other waveguide concepts require special growth or diffusion techniques. No attention, however, will be paid to waveguides **on** silicon such as silica-, oxynitride- or polymer-waveguides because these waveguides only use silicon as a substrate material but not as a material for waveguiding itself.

A. Waveguides in Epitaxial Silicon

The first integrated optical waveguides in epitaxial silicon (Fig. 3) have been proposed and fabricated in 1986 by Soref and Lorenzo [5], making use of the index step in epitaxial silicon due to different doping levels, where guiding is obtained, if the doping level of the epi-layer is lower than the doping level of the substrate. In [5], epilayers with thicknesses between $7\ \mu\text{m} \leq H \leq 43\ \mu\text{m}$ and doping levels of a few 10^{14} cm^{-3} have been used, the doping levels of the substrates were in the range of a few 10^{18} cm^{-3} up to a few 10^{19} cm^{-3}. Waveguide losses have been measured in the range of 5–13 dB/cm for slab waveguides and 15–20 dB/cm in the rib channels. These losses are due to free carrier absorption of the evanescent field in the heavily doped substrate. All these waveguides suffer from considerable losses because of the substrate absorption. However, for a sufficiently thick waveguide layer H it can be shown [6] that the losses α for the fundamental slab mode are proportional to

$$\alpha \sim \frac{1}{H^3\sqrt{N_{A,D}}} \tag{1}$$

so that combining an epi-layer with large thickness H and a very highly doped substrate the simple structure of Fig. 3 may indeed yield relatively low loss waveguides. Following these lines [6] we have achieved single mode waveguides in n/n^+-silicon with $H = 20\ \mu\text{m}, h = 13.4\ \mu\text{m}$ and $w = 12\ \mu\text{m}$, the doping levels were $N_D = 2.0 \cdot 10^{15}$ cm^{-3} and $N_D = 1.0 \cdot 10^{19}$ cm^{-3} for the epi-layer and the substrate, respectively, yielding waveguide losses between 1.2 dB/cm and 1.5 dB/cm at $\lambda = 1.3$ and $\lambda = 1.55\ \mu\text{m}$ for both, TE- and TM-polarization. Further improvement may be expected with still higher substrate doping levels.

B. Waveguides in Silicon-On-Insulator

Another material for microelectronics applications is **S**ilicon-**O**n-**I**nsulator (SOI). Optical waveguides in this material benefit from the index-step between silicon and the buried insulator (in our case SiO_2). The optical properties of SOI have been investigated by several authors, both, theoretically [7] and [8] and experimentally [9]. SOI fabrication utilizes various techniques such as **Z**one **M**elting **R**ecristallization-SOI (ZMR-SOI) [10], **S**eparation by **IM**plantation of **OX**ygen-SOI (SIMOX-SOI) [11] and **B**ond and **E**tchback-SOI (BE-SOI) [12]. The SiO_2-layer thickness in standard materials is usually in the range of a few hundred nm, the silicon top layer thickness varies in a wide range, typically 200 nm for standard SIMOX-material, up to 2 μm in standard ZMR-material and any thicknesses in BE–SOI.

The cross section of an etched rib-waveguide in SOI is shown schematically in Fig. 4, waveguiding in the vertical direction is achieved due to the high refractive-index difference between the layers of the system air–silicon–SiO_2, whereas the horizontal confinement of the optical wave is achieved by means of the etched rib. The thickness of the silicon top layer turns out to be an important design parameter with respect to the losses. The silicon top layer always contains a considerable amount of crystal-defects (10^4–10^6 cm^2), especially in case of ZMR- and SIMOX–SOI. Therefore, an additionally overgrown epi-layer yields a loss reduction due to a decreased evanescent field in the defect area, finally yielding a loss reduction following a $1/H^3$-law in case of a single mode waveguide, where H is the total top layer thickness.

Material losses Measured optical losses of SOI-waveguides are shown in Fig. 5 [13] together with the theoretical $1/H^3$-law, the curve has been fitted to the measured value at 2.9 μm as a reference. The loss values of around 0.1 dB/cm for a top-layer thickness of 11 μm are the lowest losses yet reported in singlemode silicon waveguides [14]. It can be seen, that from the loss point of view SIMOX–SOI and BE–SOI are the most useful materials, In case of ZMR–SOI, two different loss values have been measured on the same wafer: the lower value refers to measurements parallel to the observed seed-lines, whereas the higher values belong to measurements in other directions. Anyway, this material offers an optical absorption which is too high for integrated optical applications. Even though BE–SOI has the best silicon top layer quality and thus the lowest losses, a nonsatisfactory layer thickness homogeneity is observable,

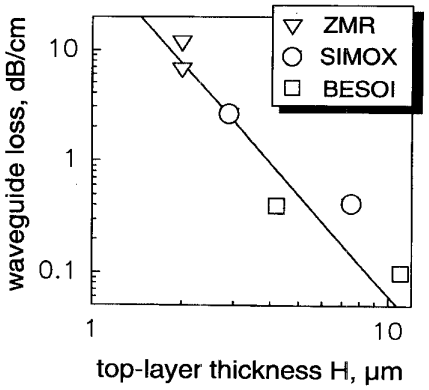

Fig. 5. Optical losses of SOI against silicon top layer thickness at $\lambda = 1.3$ μm.

therefore SIMOX–SOI still remains a promising candidate for integrated optics applications with todays technology.

1) Single-Mode Condition: Considering such relatively thick layers in conjunction with high refractive-index steps in the vertical direction, any single-mode operation seems questionnary. It is widely assumed that high refractive-index differences necessarily require submicron technology for the definition of a single-mode channel-waveguide. It has been shown in [15] and applied to SOI later in [8], that for certain rib dimensions a single-mode waveguide exists even if the corresponding slab waveguide is multimode. For waveguides with $h/H > 0.5$ no higher order vertical modes exist, since higher order vertical modes in the central region (height H) couple to the fundamental mode of the slab region (height h) with its higher effective index, thus yielding leakage losses. For single mode operation, the rib width should be

$$w \leq 0.3H_{\text{eff}} + h_{\text{eff}}/\sqrt{1-(h_{\text{eff}}/H_{\text{eff}})^2} \qquad (2)$$

where $H_{\text{eff}} \approx H$ and $h_{\text{eff}} \approx h$ denote the effective heights of the central and the slab region, respectively, accounting also for the evanescent fields. In order to prove the single-mode behavior, a BPM-simulation with a recently developed BPM-algorithm [16] has been carried out, which is able to handle even high refractive-index differences. The results of these simulations are shown in Fig. 6 for a wavelength of $\lambda = 1.3$ μm, the waveguide dimensions are $H = 4.0$ μm, $h = 2.5$ μm and $w = 4.0$ μm. The calculation at $z = 0$ is started with an input beam focussed off the axis of the rib, thus potentially coupling lots of higher modes. After a propagation length of 250 μm, higher order lateral modes are leaking away. A good stabilization of the fundamental mode can be observed after a propagation length of 2000 μm. This simulated result is in good agreement with a measured nearfield profile of a comparable rib-waveguide, which is also included in Fig. 6.

2) Waveguide Losses: Waveguides in SIMOX-material with an epitaxially thickened silicon top layer of $H = 7.4$ μm of thickness and an SiO_2-layer thickness of 0.4 μm have been investigated extensively. The rib waveguides with $h = 5.2$ μm have been fabricated by wet chemical etching, either anisotropically in KOH or isotropically in CP4. The measured waveguide losses of anisotropically etched rib waveguides are given in Fig. 7, showing optical losses of less than 0.5 dB/cm for a wide range of rib widths in the single-mode regime at $\lambda = 1.3$ μm, comparably low losses have been measured at a wavelength of $\lambda = 1.55$ μm. The measured single-mode regime in Fig. 7 is in very good agreement with (2), yielding $w \leq 9.5$ μm. More recently losses around 0.2 dB/cm have been reported with either reactive ion etched waveguide ribs [17] and [18] or isotropically etched waveguide ribs [14]. Devices based on such low loss waveguides offer attractive insertion losses if the end faces have an antireflecting Si_3N_4 coating and the waveguides are additionally tapered in order to reduce field mismatch losses. Measured insertion losses of a system standard-fiber/chip/standard-fiber of various waveguides with a total length of 60 mm are given in Fig. 8 [14] showing average insertion losses of 0.9 dB. The field mismatch losses are 0.17 dB/facet and the Fresnel losses after AR-coating are around 0.1 dB/chip giving residual waveguide losses of approx. 0.5 dB for a length of 60 mm finally yielding pure waveguide losses of less than 0.1 dB/cm.

C. Waveguides in SiGe

Germanium may be used to enhance the refractive-index of silicon. Considering a wavelength of $\lambda = 1.3$ μm, pure silicon has a refractive-index of $n_{\text{Si}} \approx 3.5$ whereas pure germanium has a refractive-index of $n_{\text{Ge}} \approx 4.3$. Following [19] and [20] with the assumption of a linear relationship between the germanium content and the refractive-index of an $Si_{1-x}Ge_x$-alloy, the refractive-index for small germanium contents may be written as

$$n_{\text{SiGe}} = n_{\text{Si}} + x \cdot (n_{\text{Ge}} - n_{\text{Si}}) \approx 3.5 + x \cdot 0.8 \qquad (3)$$

which has been found to be useful when considering indiffused waveguides. For **strained** layers a relationship between the germanium content x and the refractive-index of the layer n_{SiGe} has been found experimentally [21]

$$n_{\text{SiGe}} \approx n_{\text{Si}} + 0.3x + 0.32x^2 \qquad (4)$$

which is only based on optical measurements rather than on a physical model. Using an SiGe heterostructure with a germanium content of only a few percent yields an increase of the refractive-index which is suitable for weakly guiding structures as commonly used in integrated optics. Since the band gap shifts to longer wavelengths with increasing Ge-content, x is limited to $x \leq 0.2$ in order to avoid absorption at $\lambda = 1.3$ μm.

Germanium and silicon both belong to group IV of the periodic system, thus avoiding free carriers in a compound crystal of SiGe. Moreover, the lattice constants of both elements do not differ too much from each other, therefore also allowing epitaxial growth of thin strained SiGe-layers.

Below, we will discuss two basically different structures: rib-waveguides in grown SiGe-heterostructures (Fig. 9) and SiGe-indiffused channel waveguides (Fig. 10) (see also [22]).

1) Waveguides in SiGe-Heterostructures: Up to now, waveguides in SiGe-heterostructures have been fabricated either by MBE-[23] or CVD-growth [19] and [24]. The substrate material is a lightly doped or undoped silicon

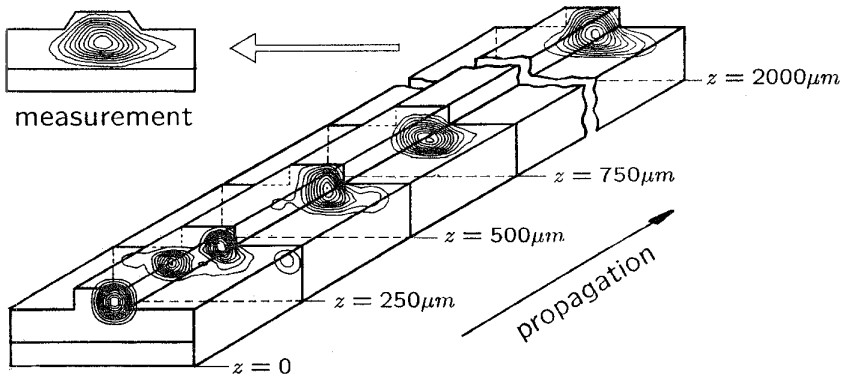

Fig. 6. BPM-simulation of a rib-waveguide with large cross section at $\lambda = 1.3$ μm.

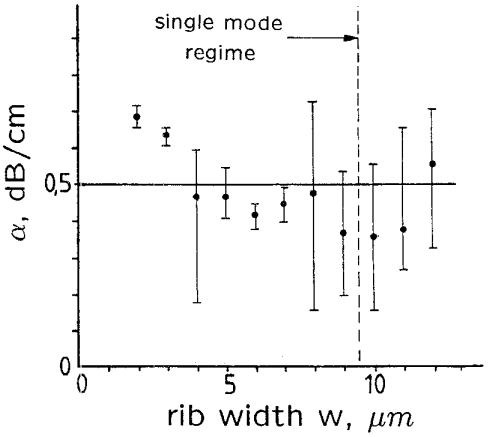

Fig. 7. Losses of SOI rib-waveguides against rib-width at $\lambda = 1.3$ μm.

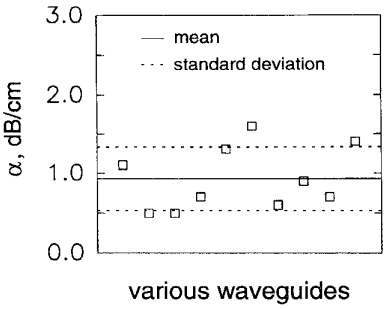

Fig. 8. Fiber/chip/fiber insertion losses of 60 mm long SOI rib-waveguides, $\lambda = 1.3$ μm.

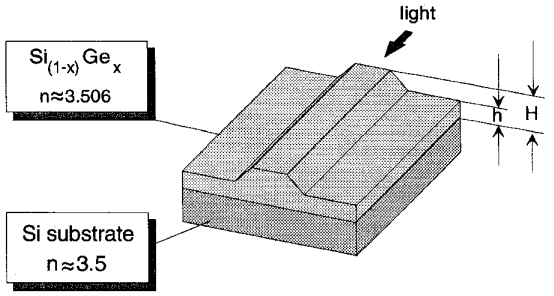

Fig. 9. Rib-waveguide in an SiGe-heterostructure.

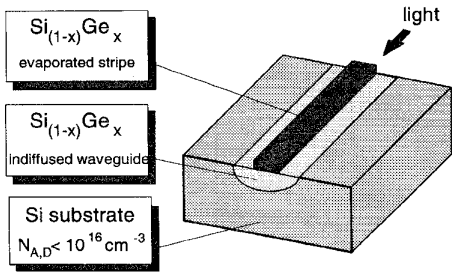

Fig. 10. SiGe-indiffused channel waveguide.

wafer. Due to the lattice-constant difference of approx. 4% between germanium and silicon, an $Si_{1-x}Ge_x$-layer can be grown dislocation free if germanium concentration and layer thickness do not exceed certain critical values, typically for layer thicknesses $\tau > 1$ μm the germanium content should be $x < 10\%$ [25] and [26].

a) MBE-grown SiGe-layers: In [23], an MBE-grown strained $Si_{0.99}Ge_{0.01}$ layer with a thickness of $H = 3.45$ μm has been used. The waveguide rib is etched anisotropically using buffered KOH, the final thickness of the $Si_{0.99}Ge_{0.01}$-layer beside the rib after etching was $h = 2.15$ μm yielding a rib-height of 1.3 μm. The width of the waveguides has been varied between 2 μm $\leq w \leq$ 12 μm. All waveguides were vertically single-moded whereas in horizontal direction single-mode behavior exists for rib-width of $w \leq 9$ μm at a wavelength of $\lambda = 1.3$ μm. From the measured mode sizes the index-enhancement has been estimated to be $\Delta n = 3.8 \cdot 10^{-3}$ which is in fairly good agreement with the value calculated from (4) for a germanium content of 1%. In [23] waveguide losses of $\alpha \approx 3$–5 dB/cm at $\lambda = 1.3$ μm have been reported. However, more recent measurements yield also loss values in the order of 1 dB/cm for MBE-grown SiGe-waveguide layers.

b) CVD-grown SiGe-layers: In [19] and [24], various CVD-grown strained and unstrained $Si_{1-x}Ge_x$ layers with x varied between 1% and 18% and thicknesses between 1 and 10 μm have been investigated. In [24], the SiGe-layer is additionally covered by a silicon layer, thus yielding a

buried waveguide. The lowest losses of the planar waveguide structures have been achieved for a 10 μm thick multimode $Si_{0.90}Ge_{0.10}$-layer, having losses of 3.2 dB/cm at TE- and 1.9 dB/cm at TM-polarization. More recently, waveguides with drastically reduced losses of 0.6 dB/cm have been fabricated at IBM [27], which also use a CVD-grown $Si_{1-x}Ge_x$-layer with a germanium content of 1.2% and a thickness of 6.5 μm with an epitaxially grown silicon top layer of 3 μm thickness, the waveguide-rib is reactively ion-etched. In addition to its low waveguide losses, these waveguides offer low coupling losses to single mode fibers since their mode profiles of 8.0 and 13.9 μm in the vertical and horizontal direction are well matched to standard single mode fibers.

2) Ge-Indiffused SiGe-Waveguides: Difficult and expensive techniques such as MBE- or CVD-growth of SiGe-layers can be avoided by simply indiffusing germanium into commercially available silicon [28] and [29]. This technique is as simple as the well known fabrication process of Ti:$LiNbO_3$-waveguides, only requiring standard technology like high-vacuum deposition, lift-off processing and diffusion. The basic idea, however, is the same as discussed above: index-enhancement by means of germanium.

Since the diffusion should take place from the solid phase, an evaporated $Si_{1-x}Ge_x$-alloy stripe has been used as a diffusion source instead of pure Ge as indicated in Fig. 10. The purpose of the alloy is an increase of the melting point of the diffusion source over that of the diffusion temperature of 1200 °C because pure germanium has a melting point as low as 937 °C. This SiGe-alloy can be fabricated e.g. by a simultaneous evaporation of silicon and germanium using two separate E-beam evaporators, with the potential of controlling the rate of both sources independently by using spectral measurement methods, i.e., **E**lectron **I**mpact **E**lectron **S**pectroscopy (EIES). Alternatively, a quasisimultaneous evaporation of silicon and germanium by means of a jumping E-beam may be used, only exhibiting an *in situ* measurement, but no *in situ* control of the alloy-ratio during evaporation. It turns out, that an $Si_{1-x}Ge_x$-alloy with $x = 0.7$ and $\tau \approx 100$–200 nm is useful as a diffusion source. In order to prevent evaporation of the SiGe-stripes during the diffusion process a SiO_2 overlay is sputtered onto the substrate before diffusion. The diffusion of the waveguides is carried out under flowing oxygen. Due to the small diffusion coefficient of germanium in silicon [30] of $D \approx 10^{-2}$ $\mu m^2/h$ at $T = 1200$ °C a diffusion time of $t_D = 65$ h at a temperature of $T = 1200$ °C is necessary, yielding a diffusion depth of $d = 1.54$ μm.

a) Refractive-index profile: Since germanium is diffused from a stripe-like source of limited thickness, the refractive-index profile of the indiffused channel is given through

$$n(x,y) = \frac{\Delta n_{\max}}{2}\left[\operatorname{erf}\left(\frac{\frac{w}{2}-y}{d}\right) + \operatorname{erf}\left(\frac{\frac{w}{2}+y}{d}\right)\right] \cdot e^{[x/d]^2} \tag{5}$$

referring to the theory of diffusion [31], where x is the vertical and y the horizontal coordinate. The waveguide parameters are the maximum refractive-index enhancement at the substrate surface $\Delta n_{\max}$, the stripe width w and the diffusion depth $d = 2\sqrt{Dt}$, which is assumed to be direction independent. Values for the maximum refractive-index enhancement dependent on the germanium content are given in Fig. 11, which have been determined from the higher order mode cut-offs, calculated by the "effective index method" [32] and [33]. These values are typically in the order of $\Delta n_{\max} \approx 10^{-1}$ and it can be seen, that they agree satisfactorily with the straight-line approximation given by (3).

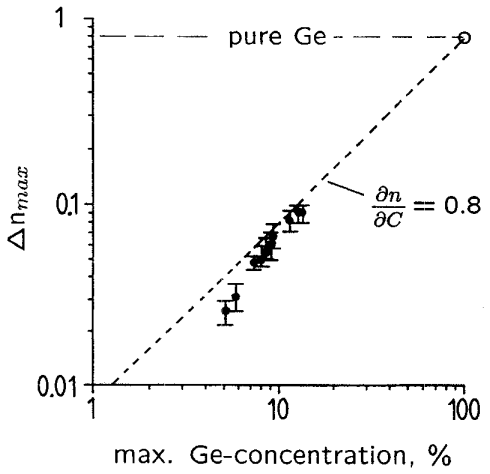

Fig. 11. Refractive-index enhancement against germanium content.

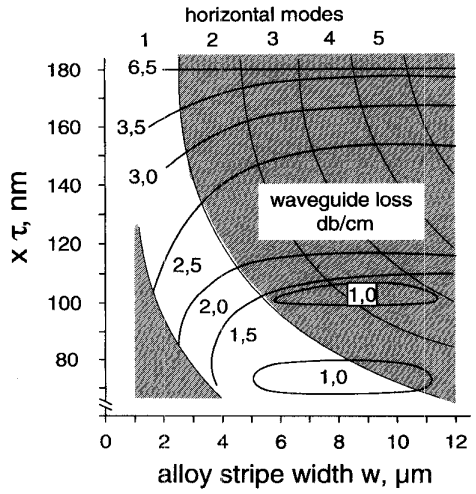

Fig. 12. Waveguide losses versus stripe-width w and $x \cdot \tau$ at $\lambda = 1.3$ μm.

b) Waveguide losses: Compared to their first proposal and the preliminary results in [28] the waveguide quality has been improved significantly, finally yielding waveguide-losses down to $\alpha \approx 0.3$ dB/cm [29]. To define the quantity of germanium to be indiffused it is likely to introduce a parameter $x \cdot \tau$. SIMS-measurements of the diffused waveguides show that all germanium from the stripe actually indiffuses to form the waveguide, where the investigated range of 69 nm $\leq x \cdot \tau \leq$ 176 nm corresponds to a maximum germanium concentration of 5% to 12.5% at the surface of the diffused waveguide. Measured loss values for a wavelength of $\lambda = 1.3$ μm are given in Fig. 12 and for $\lambda = 1.55$ μm in Fig. 13

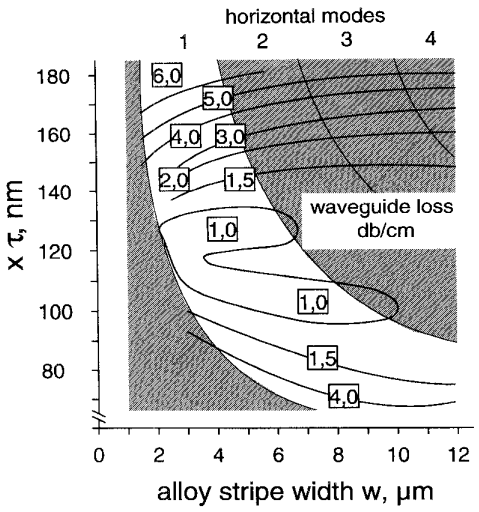

Fig. 13. Waveguide losses versus stripe-width w and $x \cdot \tau$ at $\lambda = 1.55$ μm.

[29], the lines of equal losses should be read as upper loss limits which means, that the losses within the 1 dB-ellipse are in principal lower than 1 dB. For clarification, the single mode regime is emphasized. Minimum losses of 0.3 dB/cm could be achieved at both $\lambda = 1.3$ μm and $\lambda = 1.55$ μm. The loss measurements of Figs.11 and 12 hold for TE-polarization. A comparison of the measured waveguide losses for TE- and TM-polarization at $\lambda = 1.3$ μm for three different waveguide widths is given in Fig. 14, showing a nearly polarization independent behavior.

c) Spot sizes: We have measured the horizontal and vertical $1/e^2$ spot widths as given in Fig. 15 for three different alloy-stripe widths (4, 6, and 8 μm) and a germanium quantity of $x \cdot \tau = 70$ nm. For comparison, a typical standard single-mode fiber spot of 9 μm is depicted. With the simplifying assumption of gaussian mode profiles, mode mismatch losses have been calculated, showing that mismatch losses in the order of only 1 dB/facet can be expected. III/V-waveguides with standard design parameters usually offer spot sizes in the order of 2 or 3 μm, yielding coupling losses between 6 and 10 dB/facet, which is a significantly higher coupling loss compared to indiffused waveguides in silicon.

III. Integrated Optical Components in Silicon

It is obvious that first of all passive integrated optical components in silicon are feasible, provided that the waveguides may be sufficiently bent.

In [20] losses of indiffused S-bends have been investigated at a wavelength of $\lambda = 1.3$ μm. It is evident that the bend losses strongly depend on the amount of indiffused germanium $x \cdot \tau$, which affects the mode confinement. For effective germanium concentrations of $x \cdot \tau = 70$ nm and $x \cdot \tau = 130$ nm, the bend radii should follow $R > 20$ mm and $R > 5$ mm, respectively [20], in order to avoid large bend losses. Even though these radii are large compared to radii down to few hundred μm, as can be achieved in III/V-compounds, we think that the bending performance suffices for a variety of typical

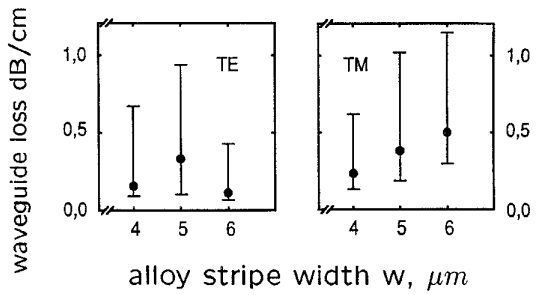

Fig. 14. Waveguide losses for Ge-indiffused waveguides for TE- and TM-polarization at $\lambda = 1.3$ μm and $x \cdot \tau = 70$ nm.

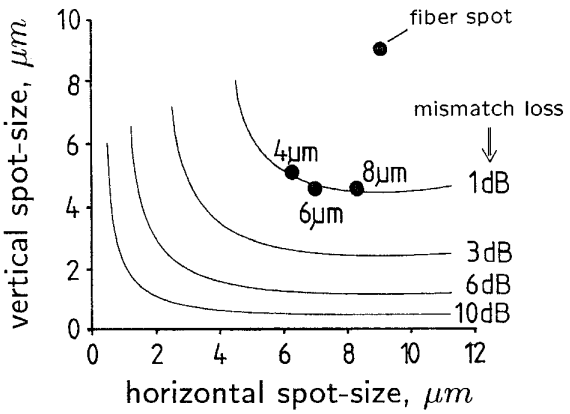

Fig. 15. Spot-widths of Ge-diffused waveguides with SiGe stripe-widths of 4, 6, and 8 μm at $\lambda = 1.3$ μm.

IO-devices. Bend losses of SOI rib waveguides at $\lambda = 1.3$ μm have been treated in [18] yielding bend radii being slightly higher than those mentioned above, which is due to a weaker lateral confinement of the optical wave in rib waveguides compared to indiffused waveguides.

A. Directional Couplers

A directional coupler is one basic component for switching and modulating purposes. Due to the fact, that the coupling properties depend on the phase-constant difference between the symmetric and asymmetric mode $\beta_{\text{symm}} - \beta_{\text{asymm}}$, directional couplers are sometimes strongly polarization dependent, especially in case of anisotropic materials. Therefore, particular attention should be paid to the polarization dependence of such devices.

In [34] and [20] Ge-indiffused directional couplers have been considered with different coupling lengths L and waveguide spacings in the coupling-region as well as with different effective germanium concentrations $x \cdot \tau$. A nearly polarization-independent operation at $\lambda = 1.3$ and $\lambda = 1.55$ μm is obtained for all these devices as illustrated in Fig. 16 for a coupler with $x \cdot \tau = 70$ nm at $\lambda = 1.55$ μm.

Directional couplers in silicon-on-insulator have been treated in [17]. These devices are fabricated on BESOI by reactive ion etching, the excess loss of the coupler is 1.9 dB at a wavelength of $\lambda = 1.55$ μm.

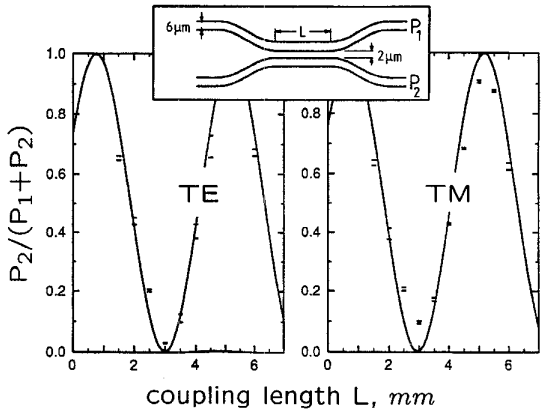

Fig. 16. Coupling properties against coupling-length for $\lambda = 1.55$ μm.

B. Waveguide/Photodetector Integration

The integration of waveguides and photodetectors is a challenging task in Si-integrated optics. Detectors for 1.3 and 1.55 μm, compatible with silicon, consist of strained thin $Si_{1-x}Ge_x$ layers, sandwiched between Si-layers in order to avoid dislocations, where x should be $x \geq 0.5$ in order to shift the bandgap of $Si_{1-x}Ge_x$ to $\lambda > 1.3$ μm [35]. Such $Si_{1-x}Ge_x$/Si-superlattices pin-photodiodes have been realized as discrete devices in [36]–[38]. Of particular interest, however, is the integration of low loss waveguides, as described above, with such photodetectors [39]–[41].

1) SOI Waveguide—SiGe Photodetector Integration: SiGe detectors may be integrated with SOI-waveguides as shown in [39]. The absorbing region is a Si/SiGe multiple quantum well pin-photodetector, the i-region consists of a 28 period superlattice of 4 nm $Si_{0.4}Ge_{0.6}$ and 21 nm Si, yielding an internal quantum efficiency of $\eta = 50\%$ at $\lambda = 1.1$ μm and 10 V reverse bias, which corresponds to an external quantum efficiency of $\eta = 12\%$, however, the quantum efficiency at $\lambda = 1.3$ μm is still rather low. The response time of the device has been measured as 200 ps, limited by the RC time constant.

2) SiGe Waveguide Photodetector Integration: A device based on SiGe-heterostructures [40] and [41] is shown in Fig. 17, which was pseudomorphically grown by MBE on ⟨100⟩-silicon. Waveguiding is obtained in a 2.5 μm-thick strained $Si_{0.98}Ge_{0.02}$-layer which is slightly p-doped ($3 \cdot 10^{17}$ cm^{-3}). In the detector region an absorbing multilayer with 700 nm total thickness is added, consisting of 20 periods 30 nm Si + 5 nm $Si_{0.55}Ge_{0.45}$. On top an undoped Si-layer with 100 nm of thickness and a 50 nm thick Si-layer with $n^+ = 10^{20}$ cm^{-3} Sb concentration are deposited. A 9 μm × 2000 μm detector rib was formed by reactive ion etching. The waveguide rib was wet chemically etched with KOH-solution. The photocurrent at $\lambda = 1.3$ μm for 80 μW optical power in a butt-coupled single mode fiber versus reverse bias voltage is shown in Fig. 18 for three different detector lengths. At a high reverse voltage an external quantum efficiency (including fiber-waveguide coupling, waveguide losses and waveguide photodetector coupling) of $\eta \approx 11\%$ has been measured as best value, corresponding to an internal efficiency of $\eta = 40\%$. Obviously, the quantum efficiency is lower at higher wavelengths, i.e. about one order of magnitude at $\lambda = 1.55$ μm. If for better quantum efficiencies at $\lambda = 1.55$ μm the germanium content is increased, fabrication problems arise due to a decreased critical thickness of the SiGe-layer. The dark current density of this device at a reverse bias of 5 V is below $1 \cdot 10^{-3}$ A/cm^2 [42]. Such a high dark current density does not seem inherent in SiGe/Si-superlattices, since recently a dark current density of $8 \cdot 10^{-8}$ A/cm^2 [38] has been reported for a discrete pin-photodiode (However, the photodiode in [38] only exhibited a 0.1% quantum efficiency at $\lambda = 1.3$ μm). Improved surface passivation should reduce the dark current also for the waveguide-photodetector combination. The frequency response of a 2 mm long photodetector has been measured with a microwave network analyzer by measuring the transmission coefficient of a system laser-fiber-photodetector. The response which is limited by the RC time constant is given in Fig. 19, showing a bandwidth of approximately 2 GHz which is due to a capacitance of $C \approx 1.7$ pF. The devices considered above use multi quantum wells that consist of periods of pure Si-layers and of SiGe-layers with a constant Ge content. This constant Ge-content can simply be described by a rectangular Ge-profile. A measurement of the time response to a power step of 600 μW at a reverse bias voltage of 2.1 V of such a device with rectangular shaped Ge-profile is given in Fig. 20. We observe a fast response with a time constant of below 1 ns, with increased time resolution this value turns out to be approx. 200 ps. This fast response is only due to the above mentioned diode's capacitance. Additionally, a slow response is observable with a time constant in the order of about 50 ns. Looking at the band diagram at reverse bias voltages it can be easily explained that the holes need some time to escape from the quantum wells due to a small energy barrier, which causes this slow response. In case of triangular shaped Ge-profiles which means that the SiGe-layers are grown with increasing Ge-content, this slow response can be avoided because now the holes can escape from the quantum wells immediately since the barrier can be totally canceled due to the tilted bands [21]. The improvement in the time response is depicted in Fig. 20, showing that the slow component is now omitted and only the fast response is observable.

3) Ultimate Performance of SiGe/Si MQW-Waveguide-Photodetectors: Based on the improved performance of triangular shaped Ge-profiles an estimate of the fundamental limits of SiGe-MQW detectors has been carried out in [43], [21], [44]. Various layer systems have been considered in order to achieve design rules and parameters for optimum quantum efficiency and bandwidth. If only moderate MQW-thicknesses of around 400 nm are allowed, a quantum efficiency of $\eta \approx 57\%$ and a bandwidth of 1.2 GHz can be achieved at $\lambda = 1.3$ μm with a 2 mm long detector region. When using MQW-thicknesses as high as approximately 2 μm the capacitance can be reduced significantly thus yielding a bandwidth of 6 GHz and an efficiency of $\eta \approx 67\%$. For $\lambda = 1.55$ μm the detector length has to be increased in order to achieve reasonable efficiencies, i.e., $l = 7$ mm. Best values hold for a MQW-thickness of approx. 2.2 μm, giving a bandwidth of 2 GHz and an efficiency of $\eta \approx 56\%$.

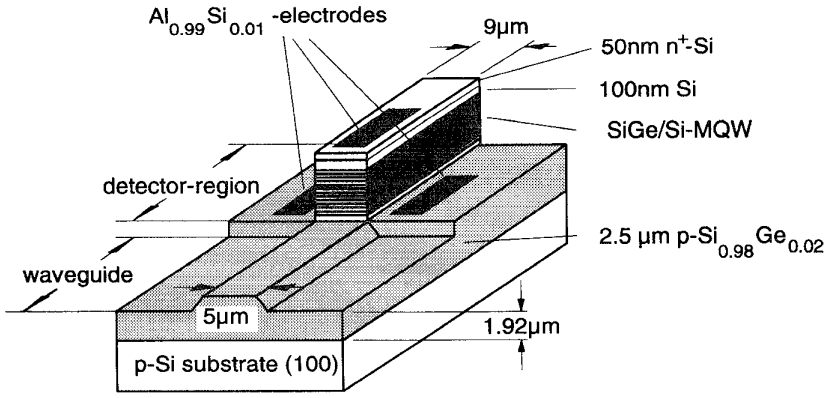

Fig. 17. Waveguide-photodetector combination for $\lambda = 1.3$ μm.

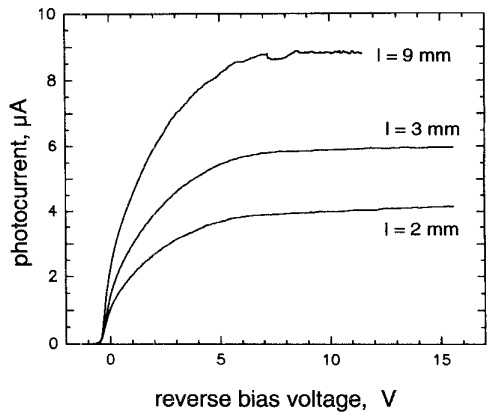

Fig. 18. Photocurrent against reverse voltage for three different detector lengths.

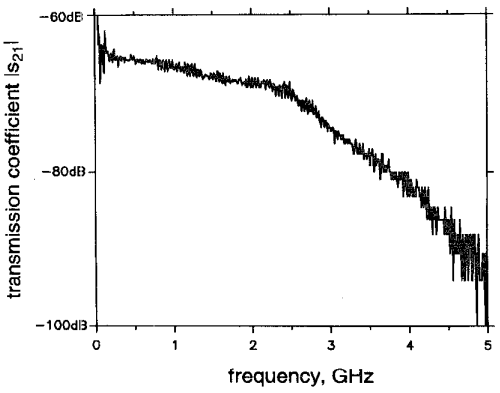

Fig. 19. Frequency response of a SiGe-waveguide/photodetector integration, absorption length $l = 2$ mm.

C. Modulators and Switches

As important as the basic requirement of an optical transparency is the existence of any electro-optic effect for modulating and switching purposes, making a material useful for integrated optics. In [45], the electro-optical effects in silicon have been summarized. Due to the symmetry properties of the crystal, no linear electro-optic (Pockels-) effect occurs in unstrained pure silicon. A second order electro-optic (Kerr)

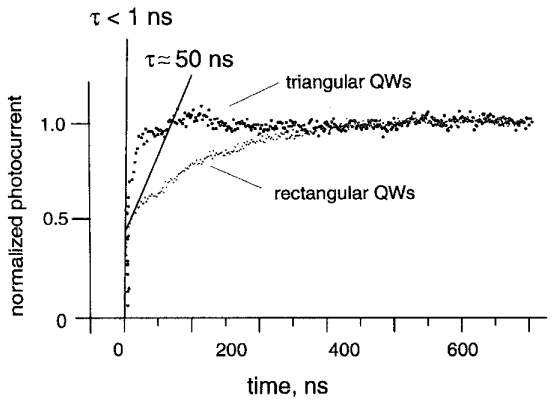

Fig. 20. Pin-photoresponse to a 600 μW step at 2.1 V reverse bias, rectangular and triangular shaped Ge-profiles.

effect is estimated in [45] yielding $\Delta n \approx 10^{-4}$ at $E = 10^6$ V/cm, which is a rather small effect. This effect has been demonstrated in amorphous silicon waveguides with a quadratic electro-optic coefficient as large as $s = 1.1 \cdot 10^{-15}$ cm^2/V^2 [46]. However, the most obvious way for an electro-optic interaction in a semiconductor material is to influence the refractive-index and/or the optical absorption by means of a carrier injection, described by the well-known relations [47]

$$\Delta n = -\frac{e^2\lambda^2}{8\pi^2 c^2 n\varepsilon_0}\left[\frac{N_e}{m^*_{ce}} + \frac{N_h}{m^*_{ch}}\right] \tag{6}$$

$$\Delta\alpha = \frac{e^3\lambda^2}{4\pi^2 c^3 n\varepsilon_0}\left[\frac{N_e}{m^{*2}_{ce}\mu_e} + \frac{N_h}{m^{*2}_{ch}\mu_h}\right] \tag{7}$$

where e is the electronic charge, ε_0 is the permittivity of free space, n is the refractive-index of silicon, m^*_{ce} and m^*_{he} are the conductivity effective masses of electrons and holes, μ_e and μ_h are the mobilities of electrons and holes, N_e and N_h are the concentrations of electrons and holes, respectively. Following [45], the results for a refractive-index change and an absorption change in silicon are given in Fig. 21(a) and (b), predicting an index change of $\Delta n \approx -10^{-4}$ at a free carrier concentration of $N = 10^{17}$ cm^{-3} and an absorption change of $\Delta\alpha \approx 1$ dB/cm at the same carrier concentration. This means, that a π-phaseshift in a Mach–Zehnder interferometer is associated

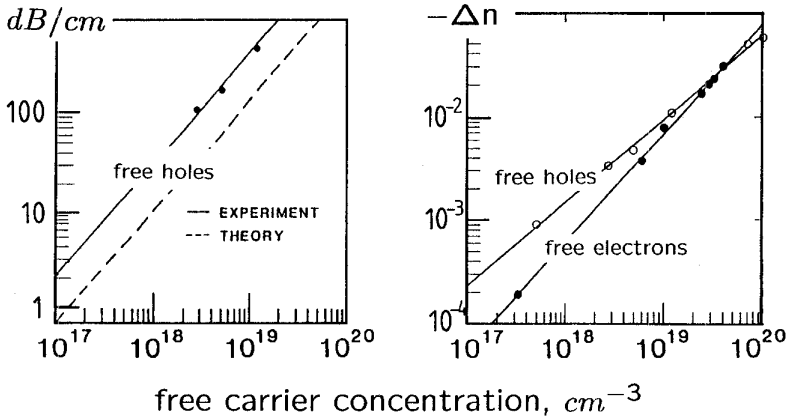

Fig. 21. Influence of free carriers at $\lambda = 1.3$ μm, (from [51]), (a) absorption and (b) refractive-index.

with an excess loss of around 1 dB. The plasma dispersion effect can be estimated from Fig. 21(b) to be $\Delta n/\Delta N \approx -1 \cdot 10^{-21}$ cm^{-3} at $N = 1 \cdot 10^{18}$ cm^{-3}.

1) Thermo-Optical Effect: Refractive-Index Change: A quite different approach for an integrated optical modulator in silicon is to make use of a thermal change of the refractive-index of silicon which is in the order of $\partial n/\partial T \approx +2{\cdot}10^{-4}/K$ [48]. Thermal modulation has been applied to a Mach–Zehnder interferometer at $\lambda = 1.3$ μm [49] where 500 μm thin film heaters were deposited on one arm of the interferometer by coevaporation of nickel and chromium. The device is fabricated on SOI, which is well suited for thermal switching due to its high thermal resistivity in the vertical direction provided by the SiO_2-layer. The material is nonstandard SOI with silicon and oxide layer thicknesses of 1.1 and 1.2 μm, respectively. With this device, a modulation depth of 40% has been demonstrated with an electrical switching power of $P \approx 60$ mW up to frequencies of $f = 10^4$ Hz. Better performance has been demonstrated at the same wavelength in [50] with a device which is also based on SOI-waveguides. The achieved modulation depth (see Fig. 22) is in the order of 3% and the bandwidth is $f = 1.6 \cdot 10^4$ Hz. In this device special attention has been devoted to an improved lateral heat confinement which is carried out by anisotropically etched V-grooves at both sides of the waveguide in the active region. Even though the bandwidth of thermo-optical devices is limited, they may be used for switching purposes, where the switching speed is of minor importance.

2) Carrier Injection: Refractive-Index Change Due to Plasma Dispersion Effect: Since any carrier injection is associated with a simultaneous heating of the injected area due to current flow, it is diffucult to demonstrate a pure plasma dispersion effect without a thermooptical modulation. Therefore, in any carrier injection experiment both effects must be separated from each other very carefully hence any injection experiment should be read very critically with respect to this fact.

In a very early work, an integrated optical multimode x-switch, based on waveguides in epi-silicon [5] was presented in [51], requiring currents of a few hundred mA, corresponding to current densities of a few kA/cm^2. Lower currents have been obtained in a bulk modulator in Si, modulating the reflected light ($\lambda = 1.3$ μm) of a single mode fiber, yielding a modulation depth of 24% for an AC current of 22 mA rms [52].

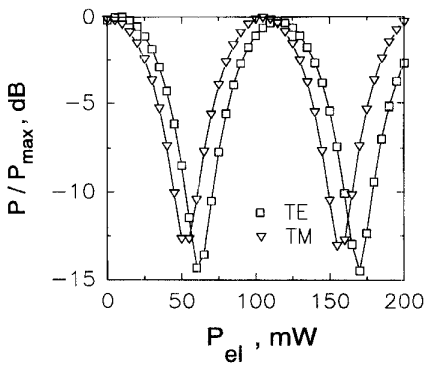

Fig. 22. Modulation characteristics of a thermo-optical Mach–Zehnder Interferometer against electrical power at $\lambda = 1.3$ μm.

In our laboratory waveguide modulators which were intentionally injection devices have been fabricated in Ge-indiffused waveguides. The diodes are designed with both, vertical and lateral pin-diodes, respectively, an example of a lateral design is given in Fig. 23 [53]. The basic material is a ⟨100⟩-oriented lightly p doped silicon substrate with a donor concentration of $N_D \approx 2 \cdot 10^{15}$ cm^{-3}, which serves as the intrinsic region of a lateral pin-diode. The n^+-doped (phosphorous) and p^+-doped (boron) areas have been fabricated by diffusion from doped spin-on glasses, yielding a maximum concentration at the surface of $N_{D\max} = N_{A\max} \approx 1 \cdot 10^{20}$ cm^{-3} and diffusion depths of 200 nm (n^+) and 700 nm (p^+), respectively. The waveguides are diffused from an amorphous SiGe-alloy with an alloy-ratio $x = 0.7$ and a thickness of $\tau = 100$ nm which corresponds to $x \cdot \tau = 70$ nm. The static modulator characteristics are given in Fig. 24(a), showing a switching characteristic dependent on the injected current which is nonsinusoidal, suggesting that the plasma dispersion effect is not dominant. Considering the modulator dependence on the electrical power [see Fig. 24(b)] it can be seen that the thermooptical effect which is proportional

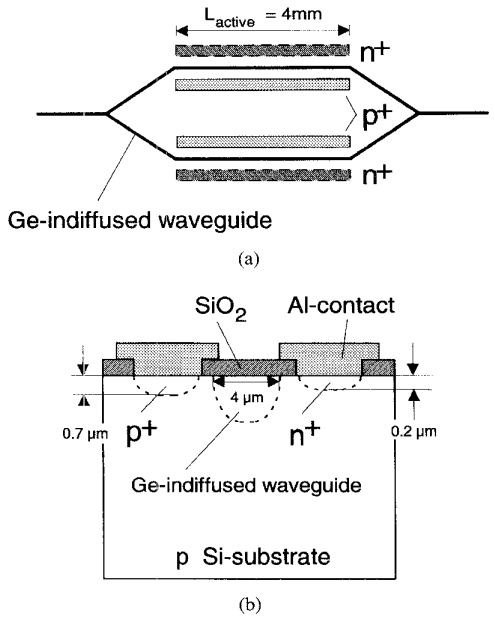

Fig. 23. Mach–Zehnder-Interferometer with Ge-indiffused waveguides. (a) Top view. (b) Cross-section of the active region.

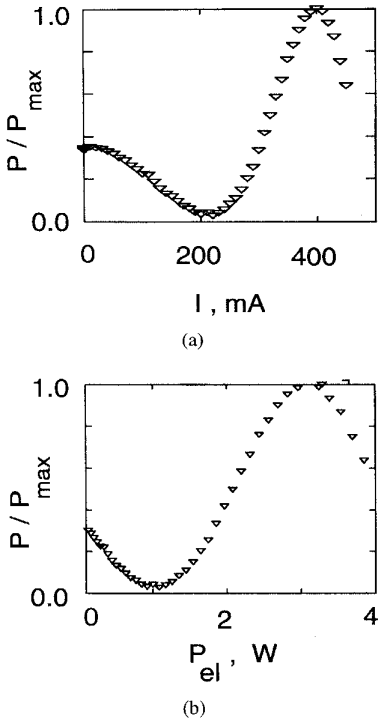

Fig. 24. Modulation characteristics of a Mach–Zehnder-Interferometer. (a) Normalized optical power against current. (b) Normalized optical power against electrical power.

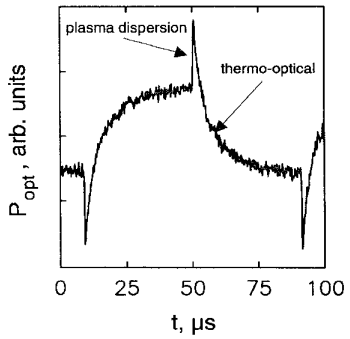

Fig. 25. Dynamic modulation characteristic.

to the electrical power dominates. In order to demonstrate the existence of the plasma dispersion effect dynamic time resolved measurements have been carried out by pulsing the injected current at a frequency of $f = 25$ kHz. The results of this measurement are given in Fig. 25 showing that both effects can be easily separated since their time constant is significantly different: the plasma dispersion effect has a fast response whereas the thermooptical effect is a rather slow process. Additionally, the different signs of $\Delta n/\Delta N$ and $\partial n/\partial T$ are verified experimentally by this measurement.

3) Carrier Injection: Absorption Change: Since a carrier injection also affects the optical absorption significantly, an optical absorption modulator based on this effect has been fabricated as a combination of a rib-waveguide and a PIN-diode [54]. The waveguide is based on the refractive-index difference in the vertical direction between a heavily doped n^+-Si-substrate and a lightly p-doped Si-layer [5] with a thickness of $H = 7.7$ μm, the rib dimensions yield a multimode waveguide in both directions. The carriers are injected by means of a vertical pin-diode. This device shows a nearly linear relationship between the current density and the absorption up to current densities of $J = 3 \cdot 10^3$ A/cm^2 where an optical absorption of around 50 dB/cm has been achieved.

IV. Micromechanics in Integrated Optics

Etching techniques in silicon can be used advantageously for self-aligned mounting of hybrid devices. It has been demonstrated in various laboratories that these techniques are feasible for integrated optics applications, especially being well suited for coupling purposes of lasers and multimode waveguides [55], lasers and singlemode waveguides [56] as well as laser-arrays with single-mode fibers [57].

Such techniques may also be used for silicon-based integrated optics as proposed in Fig. 26. It consists of a ⟨100⟩-oriented silicon micro-optical bench, only containing etched grooves for fiber-, laser- and optical chip-alignment. The optical chip, which contains integrated optical components, is mounted in a self-aligning technique upside down on the substrate. The self-aligned mounting of the chip is achieved by a rib/groove combination which is anisotropically wet etched in KOH (see Fig. 27). One major advantage of an **all silicon** realization (micro-optical bench and chip made of silicon) is an inherent balancing process that eliminates residual alignment errors due to undercutting during the etching process, if the gap between chip and micro-optical bench (Fig. 27) is wide enough. This is due to the fact, that if both elements are composed of the same crystal planes, undercutting is the

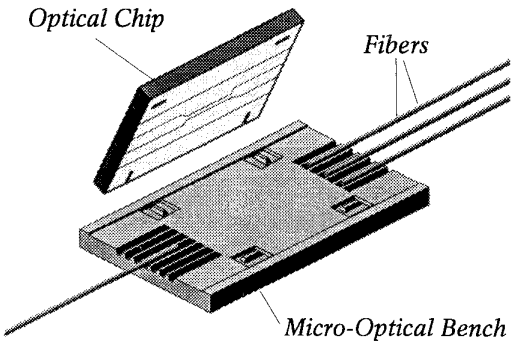

Fig. 26. Integrated optical bench using micromachined silicon.

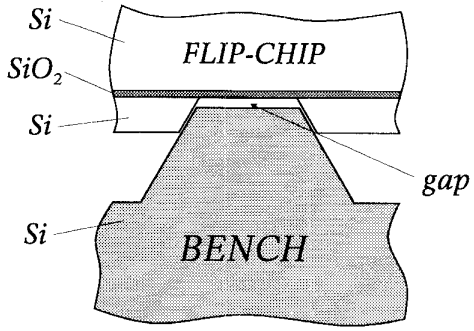

Fig. 27. Chip-bench alignment element.

same for grooves and ribs, hence only varying the above mentioned gap but not affecting the relative position of chip and bench. With this technique, the proposal of an integrated-optical receiver as given in Fig. 1 seems to be feasible. First results with straight waveguides on 4 μm BESOI yield exess losses due to misalignment in the order of 1.5 dB [58] which implies a positioning accuracy of better than 2 μm. The in- and outcoupling surfaces should be of optical quality, which is usually provided by polishing. Polishing, however, is prohibited since the length of the optical chip must be defined very precisely, i.e., with μm-precision. Therefore, cleaving the silicon crystal is a preferrable technique. The optical quality of the cleaved edge may be improved by an anisotropically wet chemically etched short V-groove in the plane to be cleaved, the depth should be around 10% of the total wafer thickness.

V. Conclusions

Various techniques and ideas have been reviewed, showing the great potential of silicon for complex integrated optical circuits. Low-loss integrated optical waveguides in silicon with losses of $\alpha < 0.5$ dB/cm have been achieved in $Si_{1-x}Ge_x$-waveguides, both, diffused and grown, as well as in rib-waveguides in SOI. These waveguide losses are comparable to those of III/V-compounds. In contrast to III/V-compounds, the waveguides are well matched to standard single-mode fibers, enabling simple and low-loss coupling. With respect to waveguide-photodetector integration an efficiency improvement by about one order of magnitude is still required which should become feasible by improved growth-techniques for SiGe. For switching, the Δn-change by carrier injection is comparable to III/V-compounds, however, the carrier lifetime in SiGe is much larger than in direct semiconductors. Switches for slow switching purposes are feasible when using the thermo-optical effect with good efficiencies especially in SOI.

Acknowledgment

The authors kindly acknowledge the help of our technical staff members: B. Kranzusch, W. Kauert, and B. Malik. The authors would also like to kindly acknowledge Kopin Corporation, SEH America, Inc., and Dr. Burbach from Fraunhofer-Institut Duisburg for providing various SOI wafers, Drs. Kasper and Presting from Daimler-Benz Forschungsinstitut Ulm for providing MBE-grown SiGe-layers, and Dr. Schlaak from Siemens AG for helpful discussions.

References

[1] B. Schüppert and K. Petermann, "Integrated optics in Si and SiGe-heterostructures," in *Proc. 18th European Conf. Opt. Commun. ECOC'92* (Invited Paper), vol. 2, pp. 793–800, 1992.
[2] R. A. Soref, "Silicon based optoelectronicss," *Proc. IEEE*, vol. 81, pp. 1687–1706, Dec. 1993.
[3] L. G. Kazovsky, "Phase- and polarization-diversity coherent optical techniques," *J. Lightwave Technol.*, vol. 7, pp. 279–292, 1989.
[4] L. D. Tzeng, W. L. Emkey, C. A. Jack, and C. A. Burrus, "Polarization insensitive coherent receiver using a double balanced optical hybrid system," *Electron. Lett.*, vol. 23, pp. 1195–1196, 1987.
[5] R. A. Soref and J. P. Lorenzo, "All-silicon active and passive guided-wave components for $\lambda = 1.3$ and 1.6 μm," *IEEE J. Quantum Electron.*, vol. QE-22, pp. 873–879, 1986.
[6] A. Splett and K. Petermann, "Low loss single-mode optical waveguides with large cross-section in standard epitaxial Silicon," *IEEE Photon. Technol. Lett.*, vol. 6, pp. 425–427, Mar. 1994.
[7] B. N. Kurdi and D. G. Hall, "Optical waveguides in oxygen-implanted buried-oxide silicon-on-insulator structures," *Opt. Lett.*, vol. 13, pp. 175–177, 1988.
[8] R. A. Soref, J. Schmidtchen, and K. Petermann, "Large single-mode rib waveguides in GeSi-Si and Si-on-SiO_2," *IEEE J. Quantum Electron.*, vol. QE-27, pp. 1971–1974, 1991.
[9] J. Schmidtchen, A. Splett, B. Schüppert, K. Petermann, and G. Burbach, "Low loss singlemode optical waveguides with large cross section in silicon-on-insulator," *Electron. Lett.*, vol. 27, pp. 1486–1488, 1991.
[10] J. C. C. Fan, M. W. Geis, and B.-Y. Tsaur, "Lateral epitaxy by seeded solidification for growth of single-crystal Si films on insulators," *Appl. Phys. Lett.*, vol. 38, no. 5, pp. 365–367, 1981.
[11] M. A. Guerra, "The status of SIMOX technology," *Solid State Technol.*, vol. 33, no. 11, pp. 75–78, 1990.
[12] W. P. Maszara, G. Goetz, A. Caviglia, and J. B. McKitterick, "Bonding of silicon wafers for silicon-on-insulator," *J. Appl. Phys.*, vol. 64, no. 10, pp. 4943–4950, 1988.
[13] T. Zinke, U. Fischer, A. Splett, B. Schüppert, and K. Petermann, "Comparison of optical waveguide losses in silicon-on-insulator," *Electron. Lett.*, vol. 29, no. 23, pp. 2031–2033, 1993.
[14] U. Fischer, T. Zinke, J.-R. Kropp, F. Arndt, and K. Petermann, "0.1 dB/cm waveguide losses in singlemode SOI rib waveguides," in *IEEE Photon. Technol. Lett.*, pp. 647–648, May 1996.
[15] K. Petermann, "Properties of optical rib-guides with large cross-section", Archiv für Elektronik und Übertragungstechnik, AEÜ, vol. 30, pp. 139–140, 1976.
[16] A. Splett, M. Majd, and K. Petermann, "A novel beam propagation method for large refractive-index steps and large propagation distances," *IEEE Photon. Technol. Lett.*, vol. 3, pp. 466–468, Aug. 1991.
[17] P. D.Trinh, S. Yegnanarayanan, and B. Jalali, "Integrated optical directional couplers in silicon-on-insulator," *Electron. Lett.*, vol. 31, pp. 2097–2098, 1995.
[18] A. G. Rickman and G. T. Reed, "Silicon-on-insulator optical rib waveguides: Loss, mode characteristics, bends and y-junctions," in *IEE Proc.-Optoelectron.*, vol. 141, no. 6, pp. 391–393, 1994.
[19] R. A. Soref, F. Namavar, and J. P. Lorenzo, "Optical waveguiding in a single-crystal layer of germanium silicon grown on silicon," *Opt. Lett.*, vol. 15, pp. 270–272, 1990.

[20] J. Schmidtchen, B. Schüppert, and K. Petermann, "Passive integrated-optical waveguide structures by Ge-diffusion in silicon," *J. Lightwave Technol.*, vol. 12, pp. 842–848, May 1994.
[21] A. Splett, "Integriert-optische Wellenleiter-Photodetektoren-Kombinationen in Silizium-Germanium-Legierungen," Ph.D. dissertation, Technische Universität Berlin, D 83, 1994.
[22] K. Petermann, J. Schmidtchen, B. Schüppert, and A. Splett, "Integrated optical waveguides in silicon," Archiv für Elektronik und Übertragungstechnik, AEÜ, vol. 45, pp. 273–278, 1991.
[23] A. Splett, J. Schmidtchen, B. Schüppert, K. Petermann, E. Kasper, and H. Kibbel, "Low loss optical ridge waveguides in a strained GeSi epitaxial layer grown on silicon," *Electron. Lett.*, vol. 26, pp. 1035–1036, 1990.
[24] F. Namavar and R. A. Soref, "Optical waveguiding in Ge_xSi_{1-x}/Si heterostructures," *J. Appl. Phys.*, vol. 70, pp. 3370–3372, 1991.
[25] R. People, "Physics and applications of Ge_xSi_{1-x}/Si strained-layer heterostructures," *IEEE J. Quantum Electron.*, vol. QE-22, pp. 1696–1710, 1986.
[26] J. C. Bean, "Recent developments in the strained layer epitaxie of germanium-silicon alloys," *J. Vac. Sci. Technol. B*, vol. 4, no. 6, pp. 1427–1429, 1986.
[27] S. F. Pesarcik, G. V. Treyz, S. S. Iyer, and J. M. Halbout, "Silicon germanium optical waveguides with 0.5 dB/cm losses for singlemode fiber optic systems," *Electron. Lett.*, vol. 28, pp. 159–160, 1992.
[28] B. Schüppert, J. Schmidtchen, and K. Petermann, "Optical channel waveguides in silicon diffused from GeSi alloy," *Electron. Lett.*, vol. 25, pp. 1500–1502, 1989.
[29] J. Schmidtchen, B. Schüppert, A. Splett, K. Petermann, "Germanium-diffused waveguides in silicon for $\lambda = 1.3$ μm and $\lambda = 1.55$ μm with losses below 0.5 dB/cm," *IEEE Photon. Technol. Lett.*, vol. 4, pp. 875–877, Aug. 1992.
[30] H. F. Wolf, *Silicon Semiconductor Data.* New York: Pergamon, 1969.
[31] J. Crank, *The Mathematics of Diffusion.* Oxford, England: Clarendon, 1986.
[32] G. B. Hocker and W. K. Burns, "Modes in diffused optical waveguides of arbitrary index profile," *IEEE J. Quantum Electron.*, vol. QE-11, pp. 270–276, June 1975.
[33] ——, "Mode dispersion in diffused channel waveguides by the effective index method," *Appl. Opt.*, vol. 16, no. 1, pp. 113–118, 1977.
[34] J. Schmidtchen, B. Schüppert, A. Splett, and K. Petermann, "Ge-diffused passive optical waveguide structures in silicon," in *Tech. Dig. Integr. Photon. Res.*, Paper TuD4, Opt. Soc. Amer., Washington, DC, vol. 7, pp. 122–123, 1992.
[35] D. V. Lang, R. People, J. C. Bean, and A. M. Sergent, "Measurement of the bandgap of Ge_xSi_{1-x}/Si strained layer heterostructures," *Appl. Phys. Lett.*, vol. 47, no. 12, pp. 1333–1335, 1985.
[36] S. Luryi, T. P. Pearsall, H. Temkin, and J. C. Bean, "Waveguide infrared photodetectors on a silicon chip," *IEEE Electron Device Lett.*, vol. EDL-7, pp. 104–107, 1986.
[37] T. P. Pearsall, H. Temkin, J. C. Bean, and S. Luryi, "Avalanche gain in Ge_xSi_{1-x}/Si infrared waveguide detectors," *IEEE Electron Device Lett.*, vol. EDL-7, pp. 330–332, 1986.
[38] B. Jalali, A. F. J. Levi, F. Ross, E. A. Fitzgerald, "SiGe waveguide photodetectors grown by rapid thermal chemical vapor deposition," *Electron. Lett.*, vol. 28, pp. 269–271, 1992.
[39] V. P. Kesan, P. G. May, E. Bassous, and S. S. Iyer, "Integrated waveguide/photodetector using Si/SiGe multiple quantum wells for long wavelength applications," in *IEDM Tech. Dig.*, 1990, pp. 637–639.
[40] A. Splett, B. Schüppert, K. Petermann, E. Kasper, H. Kibbel, and H. J. Herzog, "Waveguide/photodetector combination in SiGe for long wavelength operation," in *Tech. Dig. Series Integr. Photon. Res.*, Paper TuA4, Opt. Soc. Amer., Washington, DC, vol. 10, 1992, pp. 122–123.
[41] A. Splett, B. Schüppert, K. Petermann, E. Kasper, H. Kibbel, and H.-J. Herzog, "Waveguide/pin-photodetector combination in SiGe for long wavelength operation," OFC/IOOC Technical Digest Series, vol. 4, pp. 116–117, 1993.
[42] A. Splett, T. Zinke, K. Petermann, E. Kasper, H. Kibbel, H.-J. Herzog, H. Presting, "Integration of waveguides and photodetectors in SiGe for 1.3 μm operation", IEEE Photonics Technology Letters, PTL-6, no. 1, pp. 59–61, 1994.
[43] A. Splett and K. Petermann, "Ultimate performance of SiGe/Si-multi-quantum-well waveguide-photodetector combinations," in *Proc. ECOC'94* , vol. 1, pp. 861–864, 1994.
[44] A. Splett, Th. Zinke, B. Schüppert, K. Petermann, H. Kibbel, H.-J. Herzog, and H. Presting, "Integrated optoelectronic waveguide-detectors in SiGe for optical communications," in *SPIE'95, IMEKO Conf. Photodetectors Power Meters*, 1995, Paper 2550-11, pp. 224–324,
[45] R. A. Soref and B. R. Bennett, "Electro-optical effects in silicon," *IEEE J. Quantum Electron.*, vol. QE-23, pp. 123–129, 1987.
[46] M. Zelikson, J. Salzman, K. Weiser, and J. Kanicki, "Electro-optic effect in an amorphous silicon core waveguide structure," in *CLEO'92 Tech. Dig*, 1992, pp. 338–339.
[47] T. S. Moss, Optical Properites of Semi-Conductors. London, England: Butterworth, 1959.
[48] N. A. Nazarova, G. I. Romanova, and A. D. Yas'kov, "Refractometric characteristics of silicon," *Sov. J. Opt. Technol.*, vol. 55, pp. 220–224, 1988.
[49] G. V. Treyz, "Silicon Mach–Zehnder waveguide interferometers operating at 1.3 μm," *Electron. Lett.*, vol. 27, pp. 118–120, 1991.
[50] U. Fischer, T. Zinke, B. Schüppert, and K. Petermann, "Concepts for optical waveguide switches in silicon," in *EUROPTO'95*, Amsterdam, The Netherlands; also in "Fiber optic network components," in *Proc. SPIE 2449*, 1995, pp. 332–339.
[51] J. P. Lorenzo and R. A. Soref, "1.3 μm electro-optic silicon switch," *Appl. Phys. Lett.*, vol. 51, pp. 6–8, 1987.
[52] O. Solgaard, A. A. Godil, B. R. Hemenway, and D. M. Bloom, "Pigtailed single-mode fiber optic light modulator in silicon," *IEEE Photon. Technol. Lett.*, vol. 2, pp. 640–642, 1990.
[53] U. Fischer, B. Schüppert, and K. Petermann, "Optical waveguide switches in silicon based on Ge-indiffused waveguides," *IEEE Photon. Technol. Lett.*, vol. 6, pp. 978–980, Aug. 1994.
[54] G. V. Treyz, P. G. May, and J. M. Halbout, "Silicon optical modulators at 1.3 μm based on free-carrier absorption," *IEEE Electron Device Lett.*, vol. 12, pp. 276–278, 1991.
[55] H. Terui, Y. Yamada, M. Kawachi, and M. Kobayashi, "Hybrid integration of a laser diode and high-silica multimode optical channel waveguide on silicon," *Electron. Lett.*, vol. 21, pp. 646–648, 1985.
[56] E. E. L. Friedrich, M. G. Öberg, B. Broberg, S. Nilsson, and S. Valette, "Hybrid integration of semiconductor lasers with Si-based single-mode ridge waveguides," *J. Lightwave Technol.*, vol. 10, pp. 336–340, 1992.
[57] C. A. Armiento, M. Tabasky, C. Jagannath, T. W. Fitzgerald, C. L. Shieh, V. Barry, M. Rothman, A. Negri, P. O. Haugsjaa, and H. F. Lockwood, "Passive coupling of InGaAsP/InP laser array and singlemode fibers using silicon waferboard," *Electron. Lett.*, vol. 27, pp. 1109–1111, 1991.
[58] R. Moosburger, B. Schüppert, U. Fischer, and K. Petermann, "Passive alignment technique for all-silicon integrated optics," in *Tech. Dig. Integr. Photon. Res.*, Opt. Soc. Amer., Washington, DC, 1996, vol. 6, pp. 565–568.

Bernd Schüppert (M'95) was born in Neunkirchen, Germany, on June 5, 1947. He received the Dipl.-Ing. degree and the Dr.-Ing. degree, both in electrical engineering, from the Technische Universität Berlin, Berlin, Germany.

Since 1978, he has been a Research Associate at the Technische Universität Berlin, Institut für Hochfrequenztechnik, working on microwave-mixer problems, both theoretically and experimentally. During 1983–1984, he worked on a research project on planar balanced broadband mixers, sponsored by the Deutsche Forschungsgemeinschaft. Since 1984, he has been working on Ti:$LiNbO_3$ and more recently on silicon-integrated optics devices as a Head of the Technology Group at the Institut für Hochfrequenztechnik.

Dr. Schüppert is a member of the Verband Deutscher Elektrotechniker VDE/ITG (Germany).

Joachim Schmidtchen was born in Berlin, Germany, on August 16, 1963. He received the Dipl.Ing. degree in 1989 in electrical engineering. He received the Dr.Ing. degree in 1992 at the Technische Universität Berlin, Germany, with work based on integrated optical waveguides in silicon.

Since 1992, he has been with the Private Communication Systems branch of SIEMENS AG. In 1995, he became Project Leader for a software development project for the administration of PBX.

Armin Splett (M'93) received the Dipl.-Ing. degree in electrical engineering from the Universität Stuttgart, Germany in 1989. He received the Dr.-Ing degree from the Technische Universität Berlin, Institut für Hochfrequenztechnik in 1994.

From 1989 to 1994, he was a Research Associate at the Technische Universität Berlin, Institut für Hochfrequenztechnik. His current interests are integrated optics in silicon, novel beam propagation methods, and the role of fiber nonlinearities in optical multichannel transmission systems. Since 1994, he has been with Siemens AG, Public Communication Networks Group, where his work is concerned with wavelength division multiplexing networks.

Dr. Splett is a member of the Verband Deutscher Elektrotechniker VDE/ITG (Germany).

Uwe Fischer was born in Berlin, Germany, on May 8, 1966. He received the Dipl.-Ing. degree and the Dr.-Ing. degree, both in electrical engineering from the Technische Universität Berlin in 1991 and 1995, respectively.

From 1992 to 1996, he was a Research Associate at the Technische Universität Berlin, Institut für Hochfrequenztechnik, where he was working on SOI-based integrated optics. He is now with Siemens AG, Berlin.

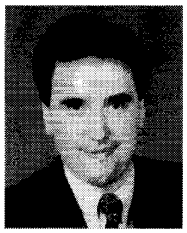

Thomas Zinke was born in Berlin, Germany, on February 24, 1966. He received the Dipl.-Phys. degree in physics from the Technische Universität Berlin, Germany, in 1991.

Since 1992, he has been a Research Associate at the Institut für Hochfrequenztechnik, Technische Universität Berlin, where his work is concerned with the integration of SOI-based passive optical components and SiGe infrared photodetectors.

Mr. Zinke is member of the Deutsche Physikalische Gesellschaft (DPG).

Rudolf Moosburger was born in Mamming, Germany, on September 13, 1967. He received the Dipl.-Ing.(FH) degree in 1991 from the Fachhochschule Regensburg and the Dipl.-Ing. degree in 1995 from the Technische Universität Berlin, both in electrical engineering.

Since 1995, he has been a Research Associate at the Institut für Hochfrequenztechnik, Technische Universität Berlin, where he is working on integrated optics in polymers on silicon.

Klaus Petermann (M'76–SM'85) was born in Mannheim, Germany, on October 2, 1951. He received the Dipl.-Phys. degree in 1974 and the Dr.-Ing. degree in 1976, both in electrical engineering from the Technische Universität Braunschweig, Germany.

From 1974 to 1976, he was a Research Associate at the Institut für Hochfrequenztechnik, Technische Universität Braunschweig, where he worked on optical waveguide theory. From 1977 to 1983, he was with AEG-Telefunken, Forschungsinstitut Ulm, Germany, where he was engaged in research work on semiconductor lasers, optical fibers, and optical fiber sensors. In 1983, he became a Full Professor at the Technische Universität Berlin, where his research interests are optical fiber communications and integrated optics.

Dr. Petermann is a member of the Optical Society of America and the Informationstechnische Gesellschaft in the Verein Deutscher Elektrotechniker (VDE).